Data in Brief 49 (2023) 109341

Contents lists available at ScienceDirect

Data in Brief

journal homepage: www.elsevier.com/locate/dib

Data Article

Dataset of optical and electronic properties for MoS_2-graphene vertical heterostructures and MoS_2-graphene-Au heterointerfaces

Sanju Gupta[a,b,**], Panagiota Pimenidou[c], Miguel Garcia[d], Shivanshi Das[e], Nicholas Dimakis[f,*]

[a] Department of Materials Science and Engineering, The Pennsylvania State University, University Park, PA 16802, (USA)
[b] Department of Physics, University of Central Florida, Orlando, FL 32816, (USA)
[c] Department of Mechanical Engineering, University of West Attica, Athens, Greece
[d] Mathematics and Science Academy, University of Texas-Rio Grande Valley, Edinburg, TX 78539, (USA)
[e] Allen High School, Allen, TX 75002, (USA)
[f] Department of Physics and Astronomy, University of Texas-Rio Grande Valley, Edinburg, TX 78539, (USA)

ARTICLE INFO

Article history:
Received 10 April 2023
Revised 29 May 2023
Accepted 20 June 2023
Available online 25 June 2023

Dataset link: graphene-MoS2-Au (Original data)

Keywords:
MoS_2/graphene/Au
Heterostructures
DFT
Band structure
Work function
Optical properties

ABSTRACT

The computational and experimental data presented in this paper refer to the research article "First-Principles Calculations Integrated with Experimental Optical and Electronic Properties for MoS_2-graphene Heterostructures and MoS_2-graphene-Au Heterointerfaces". The computational data includes structural information, electronic and optical properties, and data to calculate the work functions for various molybdenum disulfide and graphene heterostructures and their heterointerfaces with gold. The optical properties calculations include the frequency-dependent dielectric function, the refractive index, the reflectivity, the extinction coefficient, and the energy loss function. These properties were calculated using the independent particle approximation (IPA). As for the experimental optoelectronic properties, we measured photoluminescence spectra (optical), Raman spectra (vibrational), work function (surface electronic property), and local

DOI of original article: 10.1016/j.apsusc.2023.156948
* Corresponding author.
** Corresponding author at: Department of Materials Science and Engineering, The Pennsylvania State University, University Park, PA 16802, (USA).
E-mail addresses: sgup77@gmail.com (S. Gupta), Nicholas.dimakis@utrgv.edu (N. Dimakis).

https://doi.org/10.1016/j.dib.2023.109341

photoconductivity (semiconducting behavior) of graphene-MoS_2 heterointerfaces in addition to individual graphene and MoS_2 layers on gold. The variation in the exciton bands, the Raman bands, and in the average work function elucidated the semiconducting n-p junction behavior.

Specifications Table

Subject	Physics, Chemistry
Specific subject area	Computational Chemistry, Material Science
Type of data	Figure Table
How the data were acquired	The VASP program was used for all computational calculations and run at the TACC Stampede2 and Lonestar supercomputers. Experimentally, the flake identification morphology was imaged using SEM. The confocal optical and Raman spectra, the surface work function, and the local photoconductivity of the heterostructures were measured via the AFM-Raman spectrometer LabRAM HR EVOlution and the SmartSPM 1000 scope, Horiba Scientific, NJ, USA, which uses the LabSpec6 and AIST3.5 software to acquire the data.
Data format	Raw Data Analyzed
Description of data collection	Computationally, optimal geometries, electronic formation, and work function data were collected using periodic DFT. Optical properties data were collected using the independent particle approximation (IPA). The electronic band structure and densities of states, as well as the optical properties were extracted from VASP output using the vaspkit code. Experimental Raman and photoluminescence spectra were measured between 100-900 cm^{-1} (and 1.7-2.1 eV) with spectral resolution <1 cm^{-1} (5 meV) obtained using 1800 gr/mm (and 300 gr/mm) grating and analyzed using the LabSpec6 software. The atomic force microscopy (AFM), Kelvin probe force microscopy (KPFM), and conductive AFM (C-AFM) measurements operate in tapping or AC-mode and contact mode, respectively. For all tip-related measurements, Au-coated OMNI-TERS probes (APP Nano) were used. Photoconductivity measurements were made in dark (OFF) and under illumination (ON) with 633 nm laser of different intensities (0.05%, 0.1%, 1.0%, and 3.2% or power densities 0.45 kW/cm^2, 4.5 kW/cm^2, 45 kW/cm^2 and 0.14 MW/cm^2). The tip was biased, and the sample was connected to 10 MΩ series resistance. I–V curves were collected and averaged for photo-response.
Data source location	• Institution: University of Texas Rio Grande Valley • City/Town/Region: Edinburg, TX Country: USA • Institution: University of Central Florida • City/Town/Region: Orlando, FL Country: USA
Data accessibility	Repository name: Mendeley Data Data identification number: 10.17632/d62m58zt2t.1 Direct URL to data: https://doi.org/10.17632/d62m58zt2t.1
Related research article	S.Gupta, P. Pimenidou, M. Garcia, S. Das, N. Dimakis, First-principles calculations integrated with experimental optical and electronic properties for MoS_2-graphene heterostructures and MoS_2-graphene-Au heterointerfaces, Appl. Surf. Sci., 623 (2023) 156948 [1]. https://doi.org/10.1016/j.apsusc.2023.156948

Value of the Data

- We provide density functional theory (DFT) structural, electronic, and optical properties data, as well as the ones for the work functions and charge transfers of various graphene-MoS_2 heterostructures and their heterointerfaces with Au. These data are useful to material scientists for the development of 2D materials and can be used by computational chemists for further improvement.
- We report experimental data for equivalent configurations as the ones examined computationally, which verify the feasibility of our computational approach.
- These data can be used by computational material scientists and experimentalists to serve as references for comparing with calculations and measurements from corresponding defect structures.

1. Data Description

The dataset in this article describes the DFT data and the experimental data used for the calculating various properties for graphene-MoS_2 heterostructures and their heterointerfaces with Au. Figs. 1 and 2 show the frequency-dependent extinction coefficient $\kappa(\omega)$ and the energy loss function $L(\omega)$ perpendicular and parallel to the graphene (Gr) and the MoS_2 monolayer (MoS_2-1L) c axis components, respectively, for the isolated Gr, the MoS_2(1L), the Gr/MoS_2(1L) and Gr/MoS_2(1L)/Gr heterostructures, and the MoS_2(1L)/Au, MoS_2(2L)/Au, MoS_2(1L)/Gr/Au, and Gr/Au heterointerfaces. Both $\kappa(\omega)$ and $L(\omega)$ are unitless quantities. The extinction coefficient follows the profile of the imaginary part of the dielectric function for all configurations of this work. The energy loss function low values in the visible shows that the loss power is small in this energy region. The $L(\omega)$ peaks show the plasmon oscillations and the corresponding high peak values above 10 eV show the volume plasmon oscillations. Figs. 3 and 4 show SEM and optical microscopy images, respectively for the heterointerfaces of this work. The heterostructure SEM images clearly showed the graphene and MoS_2 layers due to intensity contrast. Likewise, the optical microscopy of individual large-area MoS_2 and graphene monolayers were used to prepare MoS_2/Gr heterostructures. Fig. 5 shows the measured confocal Raman spectra. Raman spectroscopy serves as a chemical fingerprint for 2D materials and the characteristic bands of constituent monolayers and the heterostructures are measured to elucidate the change in the band position, *albeit* marginal. Fig. 6 shows the local probe current measured using C-AFM (I–V curves). Here, we provide local photoconductivity measurements in dark (OFF) and under illumination (ON) for individual MoS_2 monolayer and of heterostructures which apparently showed formation of diode-like junction and how with increasing intensity the current magnitude increases as anticipated. Fig. 7 shows is a schematic of an energy level band diagram showing charge transfer characteristics and is provided to support the interpretation of our results.

Table 1 shows the C-C, Au-Au, and Mo-S distances for the structures of this work examined computationally, as well as the interlayer distances h for the heterostructures and heterointerfaces with Au. This table shows shifts in the parameters of the isolated Gr and MoS_2 monolayer due to the presence of additional layers in the heterostructures and due to Au in the heterointerfaces. Table 2 shows the dielectric constant, the maximum values for both the real and the imaginary parts of the dielectric function, and the static values for the refractive index, and the reflectivity for all configurations used in this work. The dielectric constant shows how good a material is as dielectric. The static refractive index shows the material's potential as antireflection coating and the static reflectivity its potential as a mirror. Table 3 shows the work function values obtained experimentally from the Kelvin probe force microscopy (KPFM) and computationally calculated using DFT. These data show the validity of the computational calculations on the work function for the materials examined here.

The submitted data are grouped in two directories, one for the experimental data and the one for the computational data. The experimental data directory contains five text files. The first

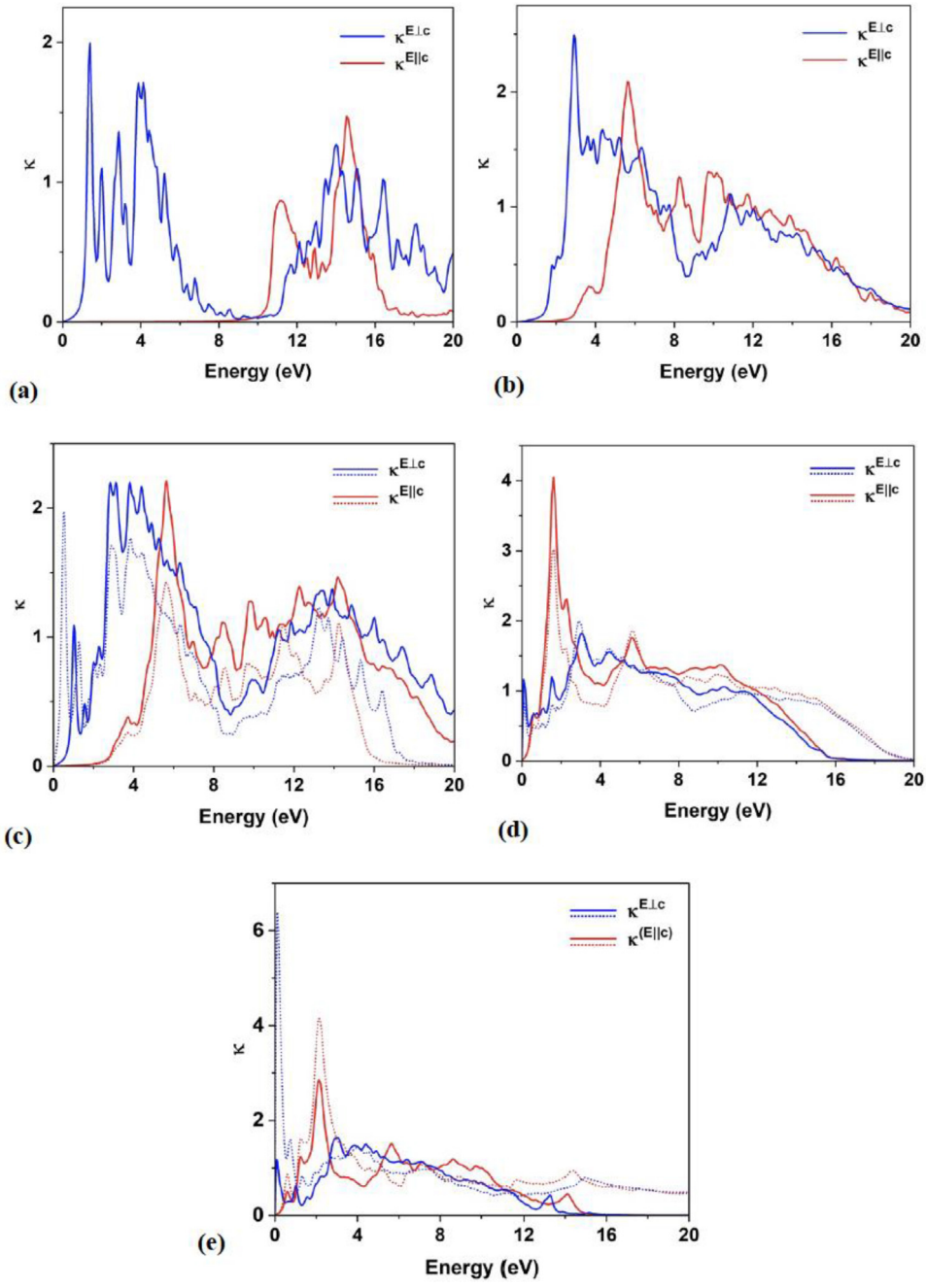

Fig. 1. The frequency-dependent extinction coefficient $\kappa(\omega)$ (unitless) perpendicular and parallel to the Gr and MoS_2(1L) *c* axis components calculated by the IPA for (a) Gr, (b) MoS_2(1L), (c) Gr/MoS_2 (solid lines) and Gr/MoS_2(1L)/Gr (dotted lines), (d) MoS_2(1L)/Au (solid lines) and MoS_2(2L)/Au (dotted lines), and (e) MoS_2/Gr/Au (solid lines) and Gr/Au (dotted lines).

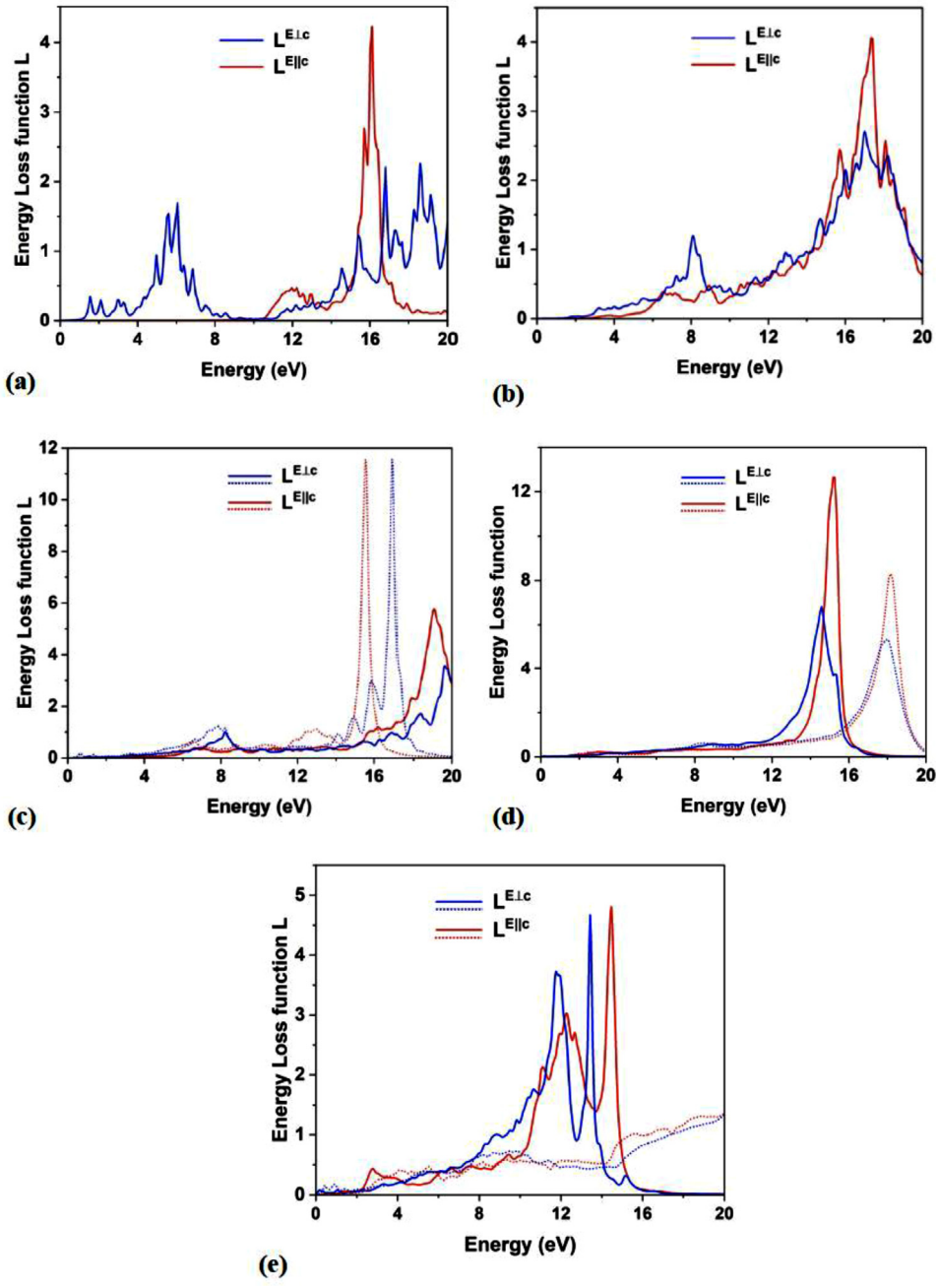

Fig. 2. The frequency-dependent energy loss function $L(\omega)$ (unitless) perpendicular and parallel to the Gr and MoS_2(1L) *c* axis components calculated by the IPA for (a) Gr, (b) MoS_2(1L), (c) Gr/MoS_2 (solid lines) and Gr/MoS_2(1L)/Gr (dotted lines), (d) MoS_2(1L)/Au (solid lines) and MoS_2(2L)/Au (dotted lines), and (e) MoS_2/Gr/Au (solid lines) and Gr/Au (dotted lines).

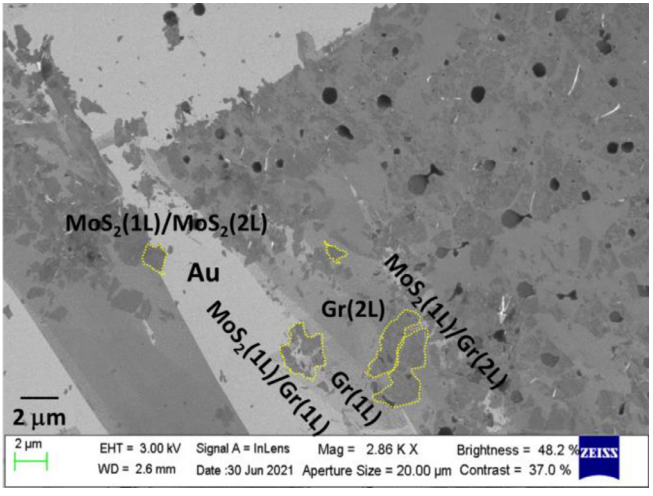

Fig. 3. SEM microscopy image showing graphene and MoS_2 surface and interface contrast.

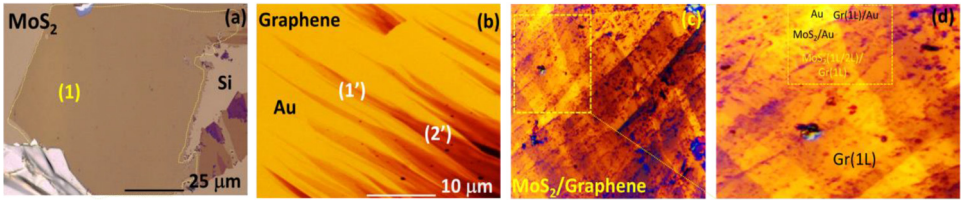

Fig. 4. Optical microscopy image of large-area MoS_2(1L)/Au, Gr/Au, and MoS_2/Gr/Au heterostructures.

Table 1
The C-C, Au-Au, and Mo-S distances for Gr, MoS_2(1L), MoS_2(1L-2L)/Au, Gr/Au, MoS_2(1L)/Gr/Au, Gr/MoS_2(1L), and Gr/MoS_2(1L), as well as the interlayer distances h for the heterostructures and heterointerfaces. The atoms distances were calculated using the VESTA [2] graphical user interface.

	Distances (Å)			
System	C-C	Au-Au	Mo-S	h
Gr	1.425			
MoS_2(1L)		2.899	2.413	
MoS_2(1L)/Au		2.810–2.921	2.403–2.417	2.67
MoS_2(2L)/Au		2.810–2.957	2.407–2.416	2.67[1]; 3.60[2]
Gr/Au	1.442	2.884		3.43
MoS_2(1L)/Gr/Au	1.452	2.881–2.884	2.401	3.40[3]; 3.41[4]
Gr/MoS_2(1L)	1.449		2.401	3.45
Gr/MoS_2(1L)/Gr	1.449		2.401	3.43

Distances between [1]MoS_2 layers, MoS_2(1L) and Au, [3]MoS_2(1L) and Gr, and [4]Gr and Au.

file is the absorption data for graphene and quasi graphene (i.e., a few layers graphene), for the MoS_2 monolayer, for the MoS_2 and graphene, and for MoS_2 and quasi graphene. The second file is the photoluminescence data for MoS_2(1L-2L)/Au, MoS_2(1L)/Gr/Au, and Gr/MoS_2(1L)/Gr/Au, and the third file is the histogram data for MoS_2. The fourth and the fifth files contain the Raman data. The computational data directory contains the processed data for band structure and DOS calculations, the VASP input and output files for the optical properties, the work function, and the atom charges, as well as the processed data for the optical properties calculations for each structure computationally examined here. The optical properties processed data contain

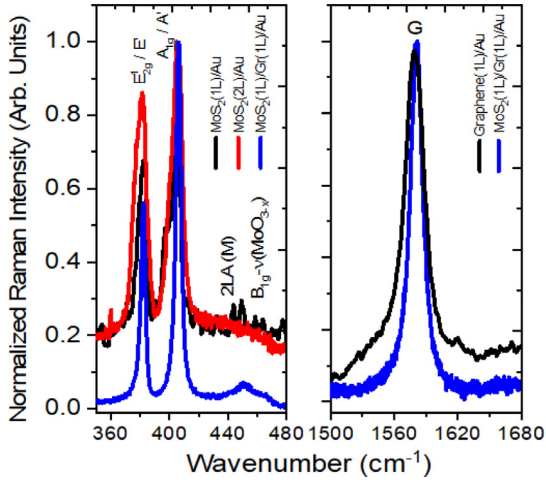

Fig. 5. Representative confocal Raman spectra measured using the 633 nm excitation wavelength showing prominent bands associated with MoS_2 ($E_{2g}{}^1$, A_{1g}), graphene (Gr) and heterointerfaces.

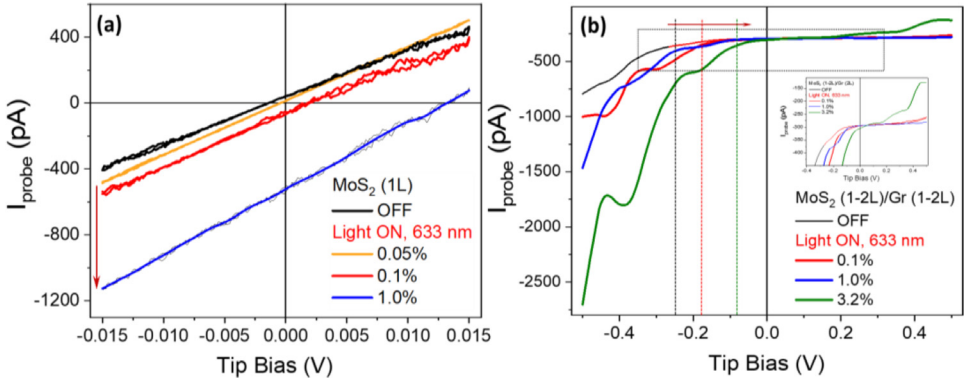

Fig. 6. Local probe current measured using C-AFM as I–V curves. (a) MoS_2/Au heterointerface and (b) MoS_2/graphene vertical heterostructures, with and without light showing n-type behavior for MoS_2/Au and rectification behavior for MoS_2(n)/graphene(p) heterointerfaces. The inset in (b) shows the zoomed area in dotted rectangle.

Table 2
The DFT calculated dielectric constant ($\varepsilon_R(0)$), the maximum values for both the real and the imaginary parts of the dielectric function ($\varepsilon_R(\omega)_{max}$ and $\varepsilon_I(\omega)_{max}$), and the static values for the refractive index ($n(0)$) and the reflectivity ($R(0)$) per unit cell configuration. For each property, the first value refers to its perpendicular component relative to the *c* axis of the Gr and MoS_2 (1L) and the second value to its parallel component.

	Property				
System	$\varepsilon_R(0)$	$\varepsilon_R(\omega)_{max}$	$\varepsilon_I(\omega)_{max}$	$n(0)$	$R(0)$
Gr	5.74; 1.62	10.12;4.27	10.91;3.75	2.40;1.27	16.89;1.41
MoS_2(1L)	7.15; 4.00	12.57; 7.62	14.92;9.70	2.67; 2.00	20.75;11.10
MoS_2(1L)/Au	25.32; 18.63	14.70; 8.35	8.96; 32.30	5.03; 4.32	44.68; 38.91
MoS_2(2L)/Au	19.21; 14.39	19.02; 17.23	11.16;20.35	4.38; 3.79	39.50; 33.96
Gr/Au	171.58; 16.26	171.58;19.86	109.34; 20.09	13.10; 4.03	73.64; 36.31
MoS_2(1L)/Gr/Au	19.64; 10.00	19.21; 12.65	7.96; 14.82	4.43; 3.16	39.92; 26.99
Gr/MoS_2(1L)	10.63; 4.51	14.81; 8.23	15.63; 10.30	3.26; 2.12	28.15; 12.96
Gr/MoS_2(1L)/Gr	12.46;	15.14; 4.51	12.72; 4.92	3.53; 1.67	31.19; 6.34

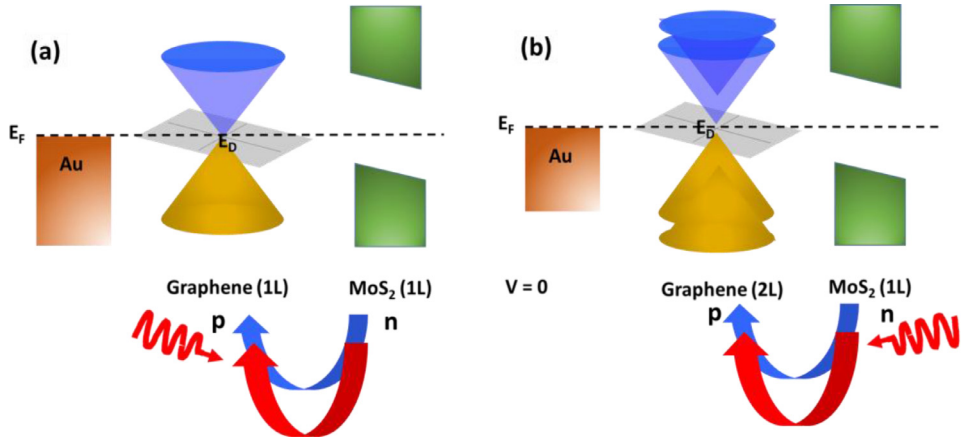

Fig. 7. Energy band diagrams at equilibrium (V=0) for MoS_2/graphene (1L and 2L)/Au heterostructure interfaces before contact where E_F is the Fermi level and E_D the Dirac point for graphene. The arrows show electron transfer from MoS_2 (n) to graphene (p) and the level increases under 633 nm (E_L=1.95 eV) illumination.

Table 3
Variation of work function values determined experimentally from Kelvin probe force microscopy (KPFM) using Au coated on SiO_2/Si and the DFT calculated counterparts, as appear in Ref. [1]. A good agreement is found between the experimentally measured and computational calculated work function.

	Work Function (eV)	
System	Experimental	Calculated
MoS_2 (1L)	4.994 ± 0.006	4.930
MoS_2 (2L)	4.962±0.005	4.951
Gr (1L)	5.050+0.011	5.035
MoS_2(1L)/Gr(1L)	4.985±0.011	5.122
Gr(1L)/MoS_2(1L)	4.623±0.008	4.542
Gr(1L)/MoS_2(1L)/Gr(1L)	4.560±0.011	4.447

information on the real and imaginary parts of the dielectric function, the refractive index, the extinction coefficient, the reflectivity, and the energy loss function.

2. Objective

This dataset can be used by computational material scientists to reproduce the electronic and optical properties calculations, as well as the atom charges and the work functions for the graphene and MoS_2 heterostructures and heterointerfaces with Au. Specifically, they can explore how the input parameters affected the accuracy of the above calculated properties. The optical properties data, calculated using the independent particle approximation (IPA), can be compared with data from more accurate approaches, such as the random phase approximation (RPA), if future computer hardware can support it. The experimental data can serve as reference data for comparison with the computational data, and thus determine their accuracy. Both the computational and the experimental data can be used for expanding this work to defect structures. Therefore, this dataset adds value to the published article due to the reproducibility of the data.

3. Experimental Design, Materials and Methods

Unit cell modeling: The isolated graphene was built as a 4 × 4 $P6_3/mmc$ supercell lattice with lattice constant of 9.87 Å. The same supercell and crystallographic group were used for the isolated monolayer 2H-MoS_2 (MoS_2-1L) with lattice constant 12.76 Å. For MoS_2-1L-2L)/Au, Gr/Au, and MoS_2(1L)/Gr/Au four-layer Au supercells, at the (111) crystallographic phase, were used. The 4 × 4 and 5 × 5 supercells for MoS_2 and graphene, respectively, were used for the Gr/MoS_2 and MoS_2/Gr/MoS_2 heterostructures. The selection on these supercells is to minimize the mismatch between the monolayer lattices. A similar strategy was used for the supercells' selections for the heterointerfaces with Au.

Simulations Design and Data Analysis: The periodic DFT code Vienna *Ab initio* Simulation Package (VASP) was used the electronic structure calculations and the optimal geometries of various MoS_2-graphene heterostructures and corresponding heterointerfaces with Au(111) [3–6]. The projector augmented-wave (PAW) pseudopotentials were used [7,8]. The Kohn–Sham equations were solved using the generalized gradient approximation (GGA) under the Perdew–Burke–Ernzerhof (PBE) functional [9] paired with the D3 semiempirical correction by Grimme [10], to account for van der Waals interactions. The kinetic energy cutoff for all calculations is set at 600 eV. We computed the electronic band structures as total and per atom orbital. The convergence criteria for energy self-consistent field (SCF) and geometry optimizations were set at 10^{-9} eV and 10^{-4} eV/Å per atom, respectively. The Brillouin-zone (BZ) was sampled using the Γ-centered 6 × 6 × 1 BZ grid for most of the calculations in this work. The work function Φ was obtained from the equation: Eqs. (1)–(7)

$$\Phi = E_{vaccum} - E_{Fermi} \tag{1}$$

where E_{vaccum} is obtained from the planar average potential calculations.

The Bader Charge Analysis code by Henkelman and co-workers [11–14] was used to compute the Bader-type ion charges [15]. This code scales linearly with the number of grid points and can be used by large unit cells.

The computationally calculated frequency-dependent dielectric function is written as:

$$\varepsilon(\omega) = \varepsilon_R(\omega) + i\varepsilon_I(\omega) \tag{2}$$

where $\varepsilon_R(\omega)$and $\varepsilon_I(\omega)$ are the real and imaginary parts of the dielectric function, respectively and ω is the photon energy. VASP calculates the imaginary part $\varepsilon_I(\omega)$ from the summation over the occupied and unoccupied states [16,17] and the real part from the imaginary part via Kramers-Kronig relation:

$$\varepsilon_R(\omega) = 1 + \frac{2}{\pi}\int_1^{\omega} \frac{\omega_1 \varepsilon_I\ (\omega_1) d\omega_1}{\omega_1^2 - \omega^2}. \tag{3}$$

Here, the dielectric properties are calculated with the electric field parallel and perpendicular to the crystallographic c-axis [18].

The corresponding refractive index $n(\omega)$, extinction coefficient $k(\omega)$, reflectivity $R(\omega)$, and energy loss function L(ω), are given in terms of the dielectric function:

$$n(\omega) = \frac{1}{\sqrt{2}}\left(\sqrt{[\varepsilon_R(\omega)^2 + \varepsilon_1(\omega)^2]^{\frac{1}{2}}} + \varepsilon_R(\omega)\right)^{\frac{1}{2}}, \tag{4}$$

$$k(\omega) = \frac{1}{\sqrt{2}}\left(\sqrt{[\varepsilon_R(\omega)^2 + \varepsilon_1(\omega)^2]^{\frac{1}{2}}} - \varepsilon_R(\omega)\right)^{\frac{1}{2}}, \tag{5}$$

$$R(\omega) = \left|\frac{\sqrt{\varepsilon_I(\omega) + \varepsilon_R(\omega)} - 1}{\sqrt{\varepsilon_I(\omega) + \varepsilon_R(\omega)} + 1}\right|^2 = \frac{(n(\omega) - 1)^2 + k(\omega)^2}{(n(\omega) + 1)^2 + k(\omega)^2}, \tag{6}$$

$$L(\omega) = \frac{\varepsilon_I(\omega)}{\varepsilon_I(\omega)^2 + \varepsilon_R(\omega)^2} \tag{7}$$

The optical properties are calculated using the independent particle approximation (IPA) [19]. All the calculations were run on the Texas Advanced Computer Center (TACC) supercomputer facilities, using Stampede 2 and Lonestar 6 supercomputers.

Materials and experimental methods. The vertical heterostructures of MoS_2(1L) and graphene were fabricated using an efficient dry transfer method on freshly prepared gold Au (111) coated SiO_2/Si substrates that were imaged using both the electron microscopy (SEM) and atomic force microscopy (AFM) [20]. Briefly, the Raman spectra were collected with a spectrometer system equipped with a Nd:YAG laser producing excitation wavelength of 532 nm (E_L=2.33 eV). To avoid photo-degradation, laser power was kept at $<$1 mW focused using 100x objective lens creating spot size of $\sim$1µm. The Raman and PL spectra were measured between 100-900 cm^{-1} and 1.7-2.1 eV with resolution $<$1 cm^{-1} and 5 meV, respectively. Raman spectra were used to determine the thickness of both MoS_2 and graphene layers. Nanosheets in the region that exhibited 1-2L of MoS_2 and 1-2L Gr were chosen for this experimental study. All the spectra were analyzed using LabSpec6 software where Gaussian-Lorentzian fitting procedure was used. The Raman spectra were calibrated against Si peak at 520.7 cm^{-1}.

The atomic force microscopy (AFM), Kelvin probe force microscopy (KPFM), and conductive AFM (C-AFM) measurements were acquired in tapping and contact mode, respectively. While the optical images were limited in spatial resolution, atomic force microscopy helped to visualize smaller flakes. Typically, for tip-related measurements, Au-coated probes (APP Nano) were used. For KPFM measurement, the gold tip was calibrated with freshly cleaved highly oriented pyrolytic graphite to determine work function (WF) in dual pass mode, which operates by detecting force gradient resulting in changes to the cantilever resonant frequency. The Au tip was biased at 3V and connected to a lock-in amplifier while the sample was grounded. For photoconductivity measurements, they were made with laser illumination at 633 nm (ON condition) besides dark (OFF condition). The sample was connected to 10 MΩ series resistance as load to collect the I–V curves and several signals were averaged for photo-response.

Ethics Statements

This work does not require any ethical statement.

CRediT Author Statement

Sanju Gupta: Conceptualization, Methodology, Data curation, Supervision, Validation, Writing, reviewing, and editing; **Panagiota Pimenidou:** Writing, reviewing, and editing; **Miguel Garcia**: Calculations, Validation, Writing, reviewing, and editing; **Shivanshi Das:** Calculations, Validation, Writing, reviewing, and editing; **Nicholas Dimakis**: Conceptualization, Methodology, Calculations, Supervision, Validation, Writing, reviewing, and editing.

Declaration of Competing Interest

The authors declare that they have no known competing financial interests or personal relationships that could have appeared to influence the work reported in this paper.

Data Availability

graphene-MoS2-Au (Original data) (Mendeley Data).

Acknowledgments

The author (S.G.) acknowledges Dr. S. Khondaker and Mr. A. Johnston for providing facilities and acquisition of some experimental data, respectively, while working at the University of Central Florida. The authors also acknowledge the Texas Advanced Computing Center (TACC) at The University of Texas at Austin for providing High-Performance Computing (HPC) resources that have contributed to the research results reported within this paper.

References

[1] S. Gupta, P. Pimenidou, M. Garcia, S. Das, N. Dimakis, First-principles calculations integrated with experimental optical and electronic properties for MoS_2-graphene heterostructures and MoS_2-graphene-Au heterointerfaces, Appl. Surf. Sci. 623 (2023) 156948.
[2] K. Momma, F. Izumi, VESTA 3 for three-dimensional visualization of crystal, volumetric and morphology data, J. Appl. Crystallogr. 44 (2011) 1272–1276.
[3] G. Kresse, J. Hafner, Ab initio molecular dynamics for liquid metals, Phys. Rev. B 47 (1993) 558(R)-561(R).
[4] G. Kresse, J. Hafner, Ab initio molecular-dynamics simulation of the liquid-metal–amorphous-semiconductor transition in germanium, Phys. Rev. B 49 (1994) 14251–14269.
[5] G. Kresse, J. Furthmüller, Efficiency of ab-initio total energy calculations for metals and semiconductors using a plane-wave basis set, Comput. Mater. Sci. 6 (1996) 15–50.
[6] G. Kresse, J. Furthmüller, Efficient iterative schemes for ab initio total-energy calculations using a plane-wave basis set, Phys. Rev. B 54 (1996) 11169–11186.
[7] G. Kresse, D. Joubert, From ultrasoft pseudopotentials to the projector augmented-wave method, Phys. Rev. B 59 (1999) 1758–1775.
[8] P.E. Blöchl, Projector augmented-wave method, Phys. Rev. B 50 (1994) 17953–17979.
[9] J.P. Perdew, K. Burke, M. Ernzerhof, Generalized gradient approximation made simple, Phys. Rev. Lett. 77 (1996) 3865.
[10] S. Grimme, J. Antony, S. Ehrlich, H. Krieg, A consistent and accurate ab initio parametrization of density functional dispersion correction (DFT-D) for the 94 elements H-Pu, J. Chem. Phys. 132 (2010) 154104–154119.
[11] W. Tang, E. Sanville, G. Henkelman, A grid-based Bader analysis algorithm without lattice bias, J. Phys. Condens. Matter 21 (2009) 084204.
[12] E. Sanville, S.D. Kenny, R. Smith, G. Henkelman, Improved grid-based algorithm for Bader charge allocation, J. Comput. Chem. 28 (2007) 899–908.
[13] G. Henkelman, A. Arnaldsson, H. Jónsson, A fast and robust algorithm for Bader decomposition of charge density, Comput. Mater. Sci. 36 (2006) 354–360.
[14] M. Yu, D.R. Trinkle, Accurate and efficient algorithm for Bader charge integration, J. Chem. Phys. 134 (2011) 064111.
[15] R. Bader, Atoms in Molecules: A Quantum Theory, Oxford Univ. Press, Oxford, 1990 in.
[16] A. Delin, P. Ravindran, O. Eriksson, J.M. Wills, Full-potential optical calculations of lead chalcogenides, Int. J. Quantum Chem. 69 (1998) 349–358.
[17] P. Rivera, W. Yao, X. Xu, Optical properties of TMD heterostructures, in: 2D Materials: Properties and Devices, Cambridge University Press, Cambridge, 2017, pp. 310–328.
[18] A.H. Reshak, S. Auluck, Calculated optical properties of 2H-MoS_2 intercalated with lithium, Phys. Rev. B 68 (2003) 125101.
[19] S.L. Adler, Quantum theory of the dielectric constant in real solids, Phys. Rev. 126 (1962) 413–420.
[20] S. Gupta, A. Johnston, S. Khondaker, Optoelectronic properties of MoS_2/graphene heterostructures prepared by dry transfer for light-induced energy applications, J. Electron. Mater. 51 (2022) 4257–4269.